On the application of differential phase measurements to study the zonal large scale wave structure (LSWS) in the ionospheric electron content

S. Tulasi Ram,[1,2] M. Yamamoto,[1] R. T. Tsunoda,[3] S. V. Thampi,[4] and S. Gurubaran[2]

[1]   The GNU Radio Beacon Receiver (GRBR) Network has been recently established to provide coverage of Southeast Asia and Pacific low-latitude regions, with planned extensions into the Indian and African longitude sectors. With the availability of CERTO (Coherent Electromagnetic Radio Tomography) beacon transmissions from Communication/Navigation Outage Forecasting System (C/NOFS) satellite, which is in a unique low-inclination (13°) orbit, it is now possible to study zonal large scale wave structure (LSWS) in ionospheric total electron content (TEC) with fine spatial resolution over a wide longitudinal region. An automated procedure to determine absolute TEC from relative TEC measurements for low inclination CNOFS orbits has been implemented through a simple single station procedure for initial offset estimation, which is shown to be consistent with the better established two station method and with observations from a Digisonde. The LSWS is extracted by subtracting the background variation from longitudinal variation of TEC. The upwellings of LSWS manifest as depletions in the residual TEC variations. Further, these zonal structures have been found, in general, to be aligned with geomagnetic field lines, and the scintillation patches have been found to align with the west walls of TEC depletions. This spatial alignment recapitulates the premise that the observed zonal wave-like structures in TEC are the manifestations of bottom side LSWS. Hence, the methodology presented in this paper, would prove useful in future, to study the characteristics of LSWS on a regular basis.

1. Introduction

[2]   The dual-frequency, differential phase measurements from low earth orbiting satellites (LEOS) have been extensively used to study the ionospheric total electron content (TEC) from the beginning of the space era [*Aitchison and Weekes*, 1959; *Garriott*, 1960; *Davies*, 1980]. Since the majority of LEOS that transmitted beacon signals in the past were polar (or high inclination) orbiting satellites, this technique has been widely used to study the latitudinal variation of TEC as well as tomographic imaging of latitude-altitude structure of ionospheric electron density along a given meridian. Clearly, if beacon transmitters are available on LEOS in low inclination orbits, it would be possible to derive the zonal variation of TEC as a function of longitude over a wide region with fine spatial resolution. In this scenario, C/NOFS is the first and the only LEOS with beacon transmitter onboard in the near-equatorial (13° inclination) orbit, and therefore, it provides an excellent opportunity to measure the zonal structures in TEC over equatorial and low latitudes.

[3]   The launch of C/NOFS is very opportune because of high space weather interest, particularly, on the topic of equatorial spread-F (ESF), for example to explore the initial seed processes that lead to the evolution of equatorial plasma bubbles (EPBs) that cause scintillations. There is accumulating evidence that the zonal large scale wave structure (LSWS) in the bottom side *F* region provides a basis for initial development of ESF [*Tsunoda*, 1981; *Tsunoda and White*, 1981]. These zonal structures together with pre-reversal enhancement of eastward electric field (PRE) appear to control the location and onset of ESF [*Tsunoda and White*, 1981; *Tsunoda*, 2005, 2008; *Tsunoda et al.*, 2010; *Saito and Maruyama*, 2007; *Thampi et al.*, 2009; *Abdu et al.*, 2009; *Kherani et al.*, 2009]. However, these studies are mostly case studies and general consensus about the role of LSWS on the occurrence of ESF has not yet emerged, primarily, due to lack of statistically significant number of observations. A reason for the dearth in observations of LSWS has been the inability to detect and characterize LSWS properties with

[1]RISH, Kyoto University, Uji, Japan.
[2]Equatorial Geophysical Research Laboratory, Indian Institute of Geomagnetism, Tirunelveli, India.
[3]Center for Geospace Studies, SRI International, Menlo Park, California, USA.
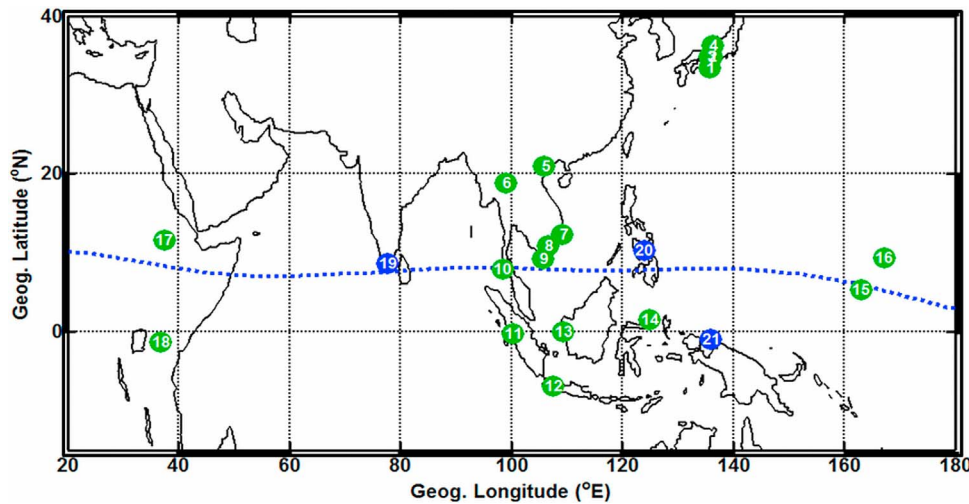[4]Physical Research Laboratory, Ahmedabad, India.

Figure 1. The geographical distribution of GRBR Network. The stations shown in green are currently installed and blue were planned for future installations.

currently available instruments, except by ALTAIR radar, a steerable incoherent scatter radar in Kwajalein Atoll.

[4] In this paper, we describe the application of differential phase technique to derive the zonal LSWS from the CERTO beacon transmissions of C/NOFS [*Bernhardt and Siefring*, 2006]. This method, for the first time, provides a simple and inexpensive means for studying the physics of these zonal structures, and should also be useful in the future, if and when more low-inclination beacon satellites become available.

2. GRBR Network

[5] A network of radio beacon receivers, namely GNU Radio Beacon Receiver (GRBR) Network, has been recently established to provide coverage of the low-latitude region. At present, GRBRs are operating in the Southeast Asia and Pacific region, with planned extensions into the other longitude sectors. A few have already been installed in Africa and others are planned for Indian region. The scientific objectives of this network are many such as three dimensional tomographic imaging of ionosphere, investigations of ionospheric scintillations and study of middle-upper atmospheric coupling processes leading to ESF. However, the scope of the present report is only confined to characterize the LSWS using radio beacon transmissions from C/NOFS. The GRBR is a compact and software controlled digital receiver optimally designed (unlike the commercially available analog receivers) to track two or more satellites simultaneously to ensure the lossless reception from all the satellites passes that are in the field of view of the receiving antenna. This is achieved by multichannel reception and careful scheduling procedures of GRBR system. To avoid multipath effects, we have set a lower limit of 20° satellite elevation angle for data acquisition. The distribution of beacon receivers is shown in Figure 1 and their station names and codes (referred in this paper), along with their geographical locations, are given in Table 1. The detailed circuitry of the receiving system and the method of TEC measurement employed in GRBR system were reported by *Yamamoto* [2008]. Further, the details of

system design and software codes are open to the community at the URL http://www.rish. kyoto-u.ac.jp/digitalbeacon/.

3. Estimation of Absolute TEC

[6] To extract the zonal LSWS, an accurate determination of absolute TEC and its variation as a function of longitude is very important. A discussion of various techniques for estimation of absolute TEC has been presented by *Bernhardt et al.* [2010]. Since the ionosphere is a dispersive medium, a radio wave passing through the ionosphere experiences an amount of group delay and phase advance that depends on the operating frequency. When two radio waves with different frequencies are transmitted, the phase difference (Φ) between the two received signals is proportional to the TEC along the line-of-sight path from the transmitter to receiver. An example of using differential group delay to obtain TEC can be found in the work by *Tsunoda and Towle* [1979]. The most commonly used satellite radio beacon frequencies have been 150 and 400 MHz, whose ratio is 3:8. For example, two radio waves at $f_1 = q_1 f_r$ and $f_2 = q_2 f_r$ (in a ratio of $q_1 : q_2$ of a common frequency f_r) are used and their phases at the receiving end are ϕ_1 and ϕ_2, then the phase difference Φ is given by

$$\Phi = \frac{\phi_2}{q_2} - \frac{\phi_1}{q_1} = \frac{40.3}{f_r c} \left[\frac{1}{q_2^2} - \frac{1}{q_1^2} \right] \int N \, dx \quad (1)$$

Here, $\int N \, dx$ is the slant (line-of-sight) TEC and c is the speed of light. The unit for TEC is generally expressed as TEC units (1 TECu = 10^{16} electrons/m^2). If it is assumed that the state of the ionosphere does not change significantly within the duration of a typical satellite pass ($\sim$10–12 min), the derived TEC variation can be assumed to be a function of satellite position. For LEOS in equatorial (or low inclination) orbits such as C/NOFS, the TEC can be derived as a function of longitude. Since the phase counting in the receiver begins from the time when the receiver acquires the phase lock with the signal, the measured phase of the radio wave at the receiver is already advanced by an unknown integer

Table 1. Low-Latitude GRBR Network

Station Number	Station Name	Station Code	Geographic Latitude	Geographic Longitude	Dip Latitude
		Currently Installed			
1	Shionomisaki	SNM	33.45	135.76	27.9
2	Shigaraki (MUR site)	MUR	34.85	136.1	29.43
3	Uji	UJI	34.90	135.8	25.53
4	Fukui	FUK	36.26	136.23	31.00
5	Phuthuy	PHT	21.03	105.96	15.75
6	Chiang Mai	CMU	18.79	98.92	13.03
7	Nha Trang	NHA	12.27	109.20	5.24
8	Ho Chi Minh City	HCM	10.85	106.56	3.52
9	Bac Lieu	BCL	9.29	105.71	1.67
10	Phuket	PTC	7.89	98.39	−0.15
11	Kototabang (EAR site)	EAR	−0.20	100.32	−9.92
12	Bandung	BDG	−6.89	107.59	−17.66
13	Pontianak	PTK	−0.00	109.36	−9.19
14	Manado	MND	1.53	124.91	−7.01
15	Kosrae	KOS	5.33	163.01	−0.5
16	Kwajalein	KWA	9.40	167.2	4.3
17	Bahirdar	BDU	11.56	37.38	3.93
18	Nairobi-KP	NKP	−1.28	36.81	−12.05
		Planned for Future Installation			
19	Tirunelveli	—	8.7	77.7	0.9
20	Cebu	—	10.35	123.91	3.09
21	Biak	—	−1.0	136	−9.68

multiples of 2π through the ionosphere which will introduce an unknown initial TEC offset (Ψ). Hence, the measured TEC is only a relative variation of slant TEC (S_r) along the direction of satellite pass. Once the unknown initial TEC offset (Ψ) is estimated, the absolute value of vertical TEC can be obtained from

$$V_a = (S_r + \Psi).\cos \chi \qquad (2)$$

where V_a is the absolute vertical TEC, S_r is the relative slant TEC, Ψ is the unknown TEC offset and χ is the satellite zenith angle at ionospheric pierce point (IPP) height. Denoting $S_r.\cos\chi = V_r$ (relative vertical TEC), then equation (2) becomes,

$$V_r = V_a - \Psi.\cos \chi \qquad (3)$$

It should be mentioned here that the equations (2) and (3) hold only during the time spans when the phases of the two radio waves have been observed continuously without any signal loss. In case of phase slips occur due to signal loss, a new Ψ must generally be used. However, these phase slips are automatically detected and resolved by appropriately shifting the slant TEC curves during the preprocessing of the data. Thus, the remaining problem in evaluating the absolute vertical TEC is the determination of initial TEC offset, Ψ.

3.1. Leitinger's Two Station Method

[7] A widely used practice for the estimation of Ψ, using the simultaneous observations from two or more closely spaced stations, was originally proposed by *Leitinger et al.* [1975]. When the two closely spaced receivers track the same satellite, it is possible that a region at the mean IPP height can be observed from both receivers (i.e., region of overlap). At a given location within the overlapping region, the ionospheric pierce points from the two receivers should be as close as possible. For polar/equatorial orbiting satellites,

the stations should be aligned along the same longitude/latitude (in other words, the longitudinal/latitudinal separation of the stations should be as small as possible). Then, it is reasonable to assume that the absolute vertical TEC (V_a) from each receiver is same at that IPP location, i.e.,

$$V_{a1} = V_{a2} \qquad (4)$$

The difference between the V_{a1} and V_{a2} should be negligible when the horizontal gradient in TEC is not too large. In this case, the vertical electron density distribution should be nearly independent of horizontal distance in the vicinity of IPP location [*Leitinger et al.*, 1975].

[8] Then from (3) $V_{r1} + \Psi_1.\cos \chi_1 = V_{r2} + \Psi_2.\cos \chi_2$ or

$$V_{r1} - V_{r2} = \Psi_2.\cos \chi_2 - \Psi_1.\cos \chi_1 \qquad (5)$$

Similarly, for n number of IPP locations within the overlapping region, one can get a system of n equations (similar to equation (5)) with different χ_1 and χ_2 as independent variables and V_{r1} and V_{r2} as dependent variables, which can be solved by least squares fit to obtain the unknown constants Ψ_1 and Ψ_2 for the two stations. Similar procedure can be extended when the observations from more than two receivers are simultaneously available [*Kersley et al.*, 1993].

3.2. Single Station Method for C/NOFS Passes

[9] For low inclination satellite passes, such as C/NOFS, the TEC variation as function of satellite position is mainly the longitudinal variation primarily due to local time or solar zenith angle variation. In addition, small variation in latitude ($\sim$3–4° for a typical pass) also introduces a gradient in the observed TEC due to the presence of Equatorial Ionization Anomaly (EIA) at low latitudes. In the presence of slowly varying ionosphere, the ionosphere itself can be considered as frozen for the duration of satellite pass (about $\sim$10–12 min). Thus, it is reasonable to assume, for the first order, that the V_a varies quasi-linearly with horizontal distance.
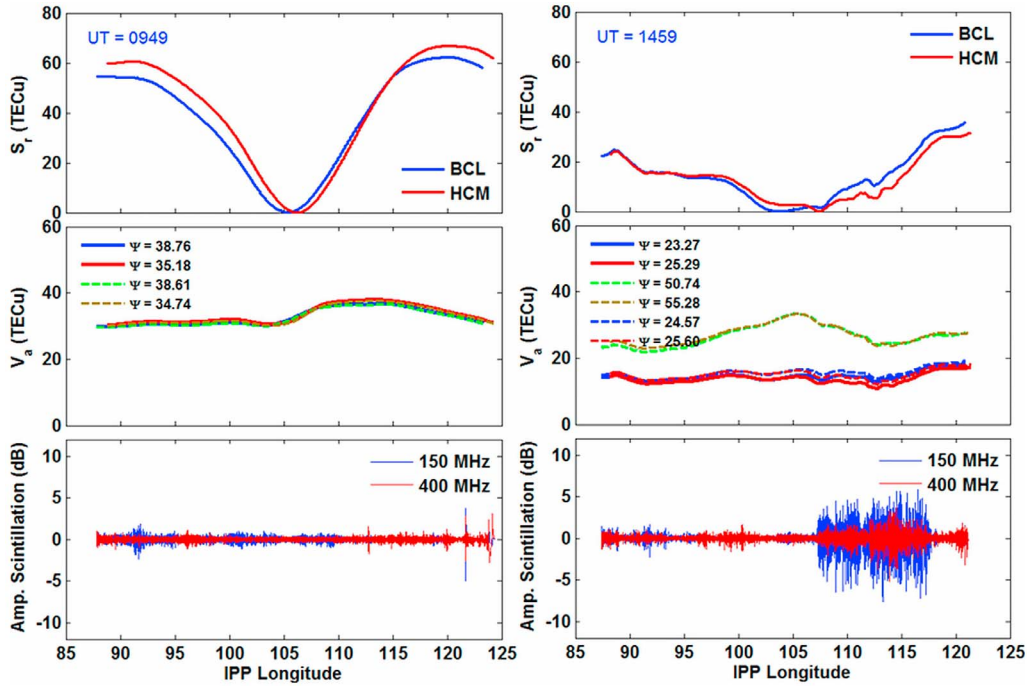
Figure 2. Comparison of estimated initial TEC offsets (Ψ) and absolute vertical TEC (V_a) derived from Leitinger's two station method and single station methods for two of C/NOFS passes at (left) 0949 UT and (right) 1459 UT on 9 March 2011. (top) The relative slant (line-of-sight) TEC observed from Bac Lieu (BCL) and Ho Chi Minh City (HCM). (middle) The V_a derived from two stations method (green and brown dotted lines for BCL and HCM, respectively) and single station method (blue and red solid lines for BCL and HCM, respectively). The V_a estimated by two station method by confining the region of overlap to 92–102°E longitudes are also shown in right middle panels (blue and red dotted lines for BCL and HCM, respectively). The unit for Ψ is TECu (10^{16} electrons/m^2). (bottom) The amplitude scintillations observed at 150 MHz (blue) and 400 MHz (red) frequency radio beacon signals from C/NOFS.

Consider that the station is at the origin of a Cartesian coordinate system in which x is eastward (zonal), y is northward and z is upward. Then the linear variation of V_a in zonal direction is given by,

$$V_a = V_a^{\chi=\chi_c} + m \cdot x, \qquad (6)$$

where χ_c is the satellite zenith angle at the closest approach. Assuming that the satellite orbits in the x-direction and the height of ionospheric pierce point is h, we have

$$\tan \chi = d/h, \qquad (7)$$

where d is the radial ground distance of ionospheric pierce point (IPP). If we define the northward ground distance of IPP at the closest approach to be y_0 at $x = 0$, then

$$\tan \chi_c = y_0/h \qquad (8)$$

Replacing y_0 in (7),

$$\tan \chi = \frac{\sqrt{x^2 + y_0^2}}{h} = \frac{\sqrt{x^2 + h^2 \cdot \tan^2 \chi_c}}{h} \qquad (9)$$

Solving for x,

$$x = h \cdot [\tan^2 \chi - \tan^2 \chi_c]^{\frac{1}{2}} \qquad (10)$$

substituting (10) in (6),

$$V_a = V_a^{\chi=\chi_c} + m \cdot h \cdot [\tan^2 \chi - \tan^2 \chi_c]^{\frac{1}{2}} \qquad (11)$$

substituting (11) in (3)

$$V_r = V_a^{\chi=\chi_c} + m \cdot h \cdot [\tan^2 \chi - \tan^2 \chi_c]^{\frac{1}{2}} - \Psi \cdot \cos \chi \qquad (12)$$

Now, the system of n equations similar to (12) with n number of χ values as an independent variables and V_r as a dependent variables, can be solved for Ψ and m by nonlinear least squares fitting. The weighted least squares fitting is used with bi-square weighting where the data points with high elevation angle are given more weight and the outliers far from the fitted line are given less weightage.

[10] Figure 2 shows the comparison of V_a estimated from both methods for two of C/NOFS orbits at 0949 and 1459 UT on March 9, 2011 over the stations Bac Lieu (BCL) and Ho Chi Minh City (HCM). The top panels show the line-of-sight TEC measured at the two stations (BCL and HCM) as a function of longitudes corresponding to an ionospheric pierce point (IPP) altitude of 300 km. Note that although the TEC variation is presented as a function of IPP longitude, its actual variation is along the IPP track that includes the latitudinal variation (though small) as well. The middle panels show the V_a derived from the observations over BCL and HCM by single station method (blue and red solid lines for

BCL and HCM, respectively) and two stations method (green and brown dotted lines for BCL and HCM, respectively). Bottom panels show the amplitude scintillations observed at 150 MHz (blue) and 400 MHz (red) frequency radio beacon signals. It can be observed from Figure 2 (middle) that the estimated V_a by the two methods are very close to each other for the C/NOFS pass at 0949 UT, indicating the TEC offset estimate (Ψ) by single station method is consistent with two-station method. However, for the C/NOFS pass at 1459 UT, the estimated values of Ψ by two-station method are much larger (50.74 and 55.28 TECu) than those obtained by single-station method (23.27 and 25.29 TECu). As can be seen from Figure 2, these larger values of Ψ obtained in two-station method manifest as an artificial enhancement in V_a over the region of closest approach due to multiplication with a factor of cos χ (equation (2)). This discrepancy between the two methods is mainly due to fluctuations in S_r around 107–118° longitudes associated with scintillation as can be seen from the bottom panels. With a view to further examine the effect of scintillations on the two station method, the TEC offsets for BCL and HCM are computed by carefully selecting the region of overlap to 92–102°E longitudes i.e., confining only to the region where the TEC observations are not affected by the scintillation. Interestingly, the resultant values for Ψ and the absolute TEC (blue and red dotted lines for BCL and HCM, respectively) are quite close to those obtained by single station method. This clearly indicates that the estimated V_a from both the methods is consistent when the measured S_r was not affected by the scintillation.

[11] It should be mentioned here that both these methods have some limitations. The single station method is subject to the assumption that the ionospheric TEC varies linearly with horizontal distance. The longitudinal extent of observation for one satellite pass is typically ~30–35°. Over this horizontal distance, the principal source of variation in TEC arises from the local time variation of about 2 to 2.3 h which can be assumed, in the first order, to be a linear variation. Further, a small latitudinal distance (3–4°) covered by the satellite pass also introduces a horizontal variation in TEC due to the presence of Equatorial Ionization Anomaly (EIA) over the low latitudes. The other sources for horizontal variation in TEC may come from the presence of ESF irregularities/plasma bubbles, medium scale traveling ionospheric disturbances, large scale wave structures, altitudinal variation of C/NOFS orbit, etc. Therefore, it is possible that the nonlinear variations introduced by the various sources are superimposed on a mean linear variation in TEC introduced by the local time/solar zenith angle variation. During our analysis for many satellite passes by solving the equation (12) by least squares fit, it is observed that the estimated coefficients (Ψ and m) are more dependent on the mean variation of TEC (trend) over the full data length and are less sensitive to the smaller scale nonlinear variations. However, the estimation of Ψ becomes ambiguous when the major portion of line-of-sight TEC data is severely affected by the scintillations. On the other hand, the two station method depends on the assumption of equality of V_a at a given IPP in the overlapping region observed by the two receivers that are separated horizontally. When the horizontal gradient of ionospheric TEC is significantly large, the line-of-sight paths between the transmitter and receivers for different stations pass through the regions with different

electron densities, and hence, the assumption of equality is violated. Therefore, the estimated value for Ψ is highly sensitive to the selection of overlapping region and often is unrealistic when the gradients are large in the overlapping region, such as due to local time variation, EIA and the presence of ESF irregularities. For the low-inclination orbiting satellite passes, such as C/NOFS, the longitudinal gradients of TEC is significant owing to the solar zenith angle variation which maximizes during the sunrise and sunset periods. Given that the resultant offset estimates by single station method are consistent with those by two station method, the single station method is invulnerable when the horizontal gradients are linear. Moreover, the single station approach is simple and practicable when the closely spaced receivers are not available. However, this method may not be suitable to derive the absolute TEC from polar (or high inclination) orbiting satellites, particularly at low latitudes, due to large gradients associated with double humped latitudinal variation of TEC introduced by EIA.

3.3. Validation of Single Station Method

[12] Figure 3 shows the longitudinal variation of V_a by single station method during nine successive C/NOFS orbits from 0815 UT to 2206 UT on May 18, 2011 over an equatorial station, Kosrae (KOS). The x axis for each panel is shown in terms of local times and the corresponding longitudes are presented in the axis at top. It can be observed from Figure 3 that the longitudinal variations of TEC in each panel are in the right sense with the local time variation, particularly, for those passes where the observations crossing the sunset and sunrise solar terminators (at 0815 UT and 1837 UT). Further, the V_a at any selected longitude is also found to decrease as the local time advances in to midnight and post-midnight hours and increases after sunrise. For example, consider a longitude at 167.2°E and the estimated V_a for the nine successive orbits are plotted as a function of local time (blue curve with open circles) in Figure 4b. This longitude sector is selected because of the availability of a Digisonde at Kwajalein (KWA) for validating the estimated TEC. The tracks of ionospheric pierce points (at 300 km) for the nine orbits are numbered 1 to 9 and the locations of KOS and KWA are shown in Figure 4a. It can be seen that the V_a exhibits a clear local time variation with decrease after sunset, reaching a minimum around 0415 LT and increase after sunrise.

[13] In order to validate the estimated V_a, the vertical electron density profiles are reconstructed up to the altitude of C/NOFS orbit by assimilating the topside in situ ion density measurements from C/NOFS Ion Velocity Meter (IVM) [*Coley et al.*, 2010] with the bottom side profiles obtained from the Digisonde. In this method, the topside ion density data points are used as an anchor point to reconstruct the topside profile using α-Chapman function which is found to be in good agreement with the incoherent scatter radar profiles and the detailed procedure can be found in the work by *Tulasi Ram et al.* [2009]. Integrating these vertical profiles provide the vertical TEC over the KWA (herein after called as ITEC) between the ground and the C/NOFS altitude and are plotted as red curve with asterisks in Figure 4b. It should be mentioned here that the V_a from beacon data (blue curve) corresponds to 167.2°E IPP longitude for all the nine C/NOFS orbits but their IPP latitudes differ for each orbit.
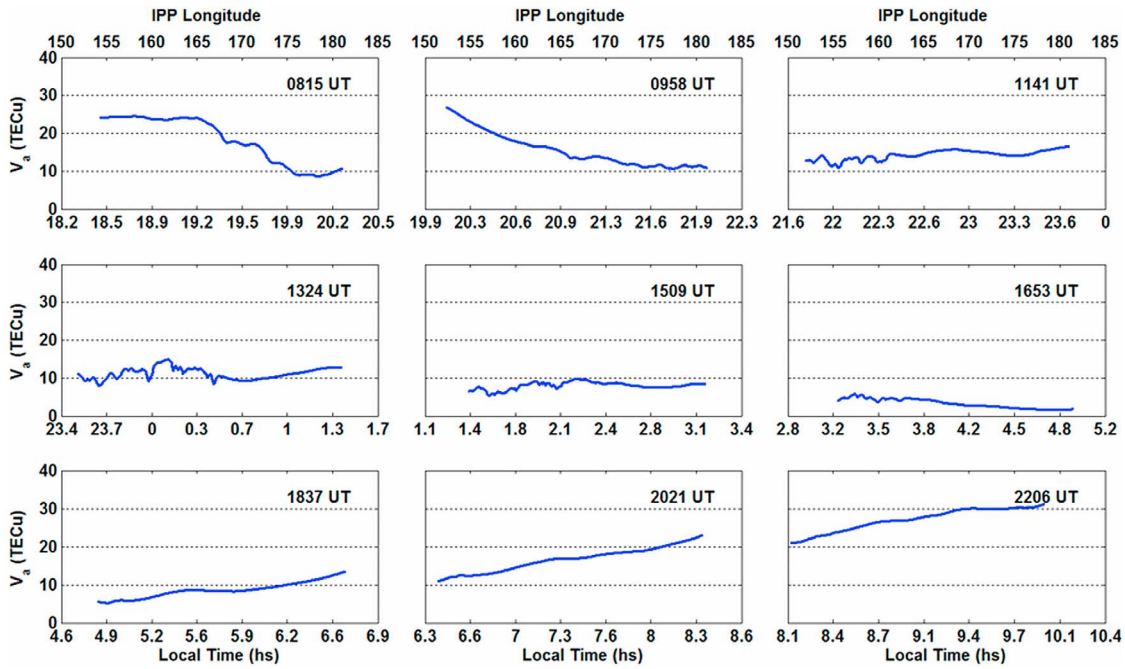
Figure 3. Longitudinal variation of V_a derived from single station method for nice successive C/NOFS orbits covering the local times from dusk to dawn on 18 May 2011 over an equatorial station, Kosrae (KOS). The x axis for each panel is shown in terms of local times corresponding to the longitudes shown at top.

Whereas the ITEC (red curve) can be considered as a vertical TEC over KWA since the bottom side density profile is obtained from the Digisonde at KWA. However, the topside anchor points of in situ data correspond to different latitudes for the nine C/NOFS orbits. Thus, the ITEC represents the true vertical TEC over KWA between the ground and C/NOFS altitude only when C/NOFS orbit is in close latitudinal proximity of KWA Digisonde. The horizontal distance between the observational locations of V_a and KWA are plotted as vertical bars with right hand side scale in Figure 4b. Therefore, the estimated V_a is expected to be close to true TEC only when the horizontal distance is small. It can be seen from Figure 4 that the V_a is close to true TEC during 0 to 6 LT, i.e., for passes numbered 4, 5, 6 and 7 when the horizontal distance is small and differ significantly as the horizontal distance increases. These features of consistent local time variation and close proximity with the true TEC over KWA further validates the accuracy of estimated V_a by single station method. Hence, we conclude that the single station method described in section 3.2 is appropriate for the estimation of absolute TEC for LEOS with low-inclination orbits, such as C/NOFS.

4. LSWS From Longitudinal Variation of TEC

[14] The longitudinal variation of TEC often exhibits zonal wave-like structures, superimposed on the background variation, which can be regarded as large scale wave structure (LSWS). *Rottger* [1973], from transequatorial propagation experiment, has reported that the ESF patches were distributed quasi-periodically in longitude and interspersed by an average zonal distance of about ~380–450 km. They have interpreted these quasiperiodic ESF structures in east-west
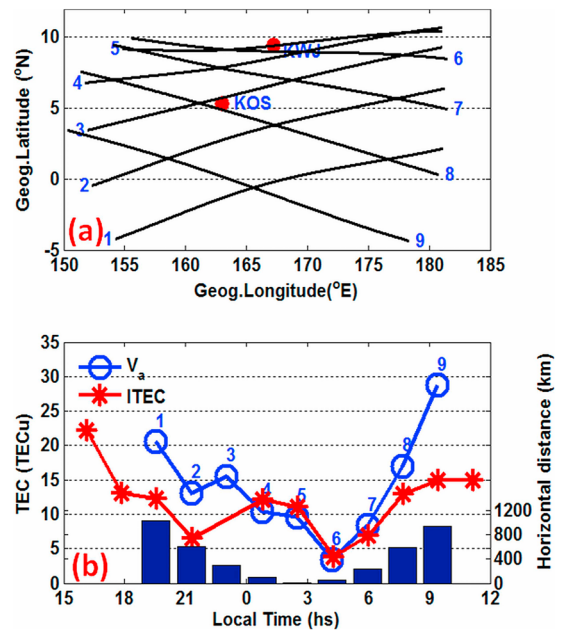

Figure 4. (a) The location of Kosrae (KOS) and Kwajalein (KWA) and the tracks of ionospheric pierce points (300 km) for nine C/NOFS orbits on 18 May 2011. (b) The local time variations of V_a (blue curve) and ITEC (red curve) corresponding to 167.2°E longitude sector. The vertical bars represent the horizontal distance (right-hand side scale) between the observational locations of V_a and KWA.
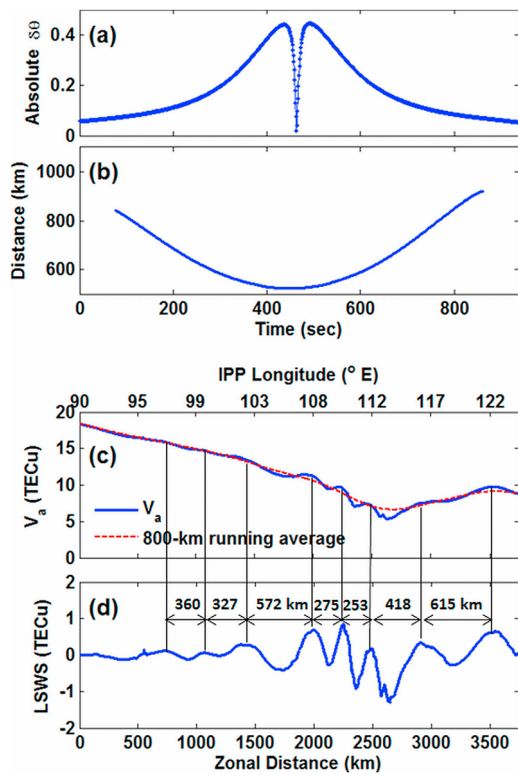
Figure 5. Derivation of LSWS from the longitudinal variation of absolute vertical TEC (V_a). (a) Absolute change in satellite elevation angle ($\delta\theta$) per 1-sample as a function of time since the beginning of data acquisition. (b) Variation of zonal distance corresponding to 2.5 min (± 1.25 min) time interval centered at that point of time. (c) Variation of V_a (blue curve) as function of zonal distance (x axis at bottom) and IPP longitude (x axis at top) and 800-km running average curve (red dashed line). (d) Residual TEC variations showing the typical zonal wavelengths of ~250–615 km.

direction to the zonal wavelengths of LSWS excited by atmospheric gravity waves. *Tsunoda and White* [1981] from ALTAIR incoherent scatter radar observations have shown that the zonal wavelengths of LSWS vary around ~300–600 km, which were later supported by satellite in situ observations by *Singh et al.* [1997]. Therefore, the variations in TEC with scale lengths greater than 800 km can be safely assumed as the background variation and may be subtracted from the longitudinal TEC variation in order to derive the zonal LSWS. *Thampi et al.* [2009] and *Tsunoda et al.* [2010] have assumed that the mean IPP location sweeps through a zonal distance of ~1000 km within 2.5 min period of observations from C/NOFS, hence computed a 2.5 min period running average of TEC and subtracted from the longitudinal TEC variation in order to derive LSWS. However, care must be taken while subtracting the running average of a uniform time interval owing to the fact that uniform time interval does not corresponds to a uniform zonal distance due to the differential variation of satellite elevation angle during different epochs of satellite pass. This is because, with respect to ground receiver, the satellite elevation angle (θ) varies slowly when the satellite is far, varies rapidly at the closest approach, and again varies slowly as the

satellite is moving away. For example, Figure 5a shows the absolute change in θ per 1-sample ($\delta\theta$) as a function of time since the beginning of data acquisition for a C/NOFS pass at 1225 UT of 26 February 2011 from an equatorial station, Bac Lieu (BCL). Figure 5b shows the variation of zonal distance that corresponds to 2.5 min (± 1.25 min) time interval centered at that point of time. It can be seen from Figure 5b that the variation in $\delta\theta$ is quite significant during the different epochs of the satellite pass and the corresponding zonal distance varies from 900 km to 500 km. Therefore, the running average of a uniform time interval is not suitable; instead one needs to subtract the running average of a uniform zonal scale size of 800 km. Hence, the process is refined here as described in the following lines. The zonal distance swept by the IPP at an altitude of 300 km computed and the variation of V_a (blue curve) as a function of zonal distance in shown in Figure 5c. The corresponding IPP longitudes are shown in the x axis at the top. It can be observed from Figure 5c that the zonal variation of V_a exhibits wave-like structures conspicuously to the east of 100°E longitude. It should be mentioned here that even though V_a curve is smooth because of fine spatial resolution, the sampling interval of zonal distance is not uniform as discussed previously. Therefore, the V_a curve is re-sampled at a uniform zonal distance of 1 km. Now the running average corresponding to 800 km is subtracted (red dashed line) from the V_a curve and the residual variations are shown in Figure 5d. While computing the 800 km running average curve (red dashed line), we applied the hamming window weighting function [*Oppenheim and Schafer*, 1989] on the data series in order to reduce the edge effects at the beginning and end of the data series. It can be seen from Figure 5d that the residual V_a exhibits zonal wave-like variations with wavelengths of ~250 to 615 km, which are consistent with the values reported for LSWS in earlier studies [*Rottger*, 1973; *Tsunoda and White*, 1981; *Singh et al.*, 1997].

5. Discussion

[15] The equatorial ionosphere often exhibits zonal wave-like structures that manifest as a quasiperiodic modulation in the height of iso-electron density contours by backscatter radar maps, which were termed as a Large Scale Wave Structure (LSWS) by *Tsunoda and White* [1981], *Tsunoda* [1981], and *Tsunoda* [2005]. They have further shown that the ESF irregularities or equatorial plasma bubbles (EPBs) grow from the upwellings or crests of LSWS. Figure 6 shows the zonal wave-like structures in the longitudinal variation of V_a simultaneously observed from three equatorial and low-latitude stations, BCL, HCM and NHA for the same C/NOFS pass as that shown in Figure 5. The top panel shows the locations of the three stations and the IPP tracks of C/NOFS pass for the three stations. The x axis at the top represents the local times corresponding to the IPP longitudes. The vertical green and red dotted lines represent the location of sunset terminator corresponding to E region (110 km) and F region (200) altitudes. The second panel (Figure 6b) shows the variation of V_a (solid lines) from the three stations as a function of IPP longitude. It can be observed from Figure 6b that the estimated V_a exhibits zonal wave-like structures for all the three stations, conspicuously to the east of 100°E longitude. The local times at the corresponding longitudes
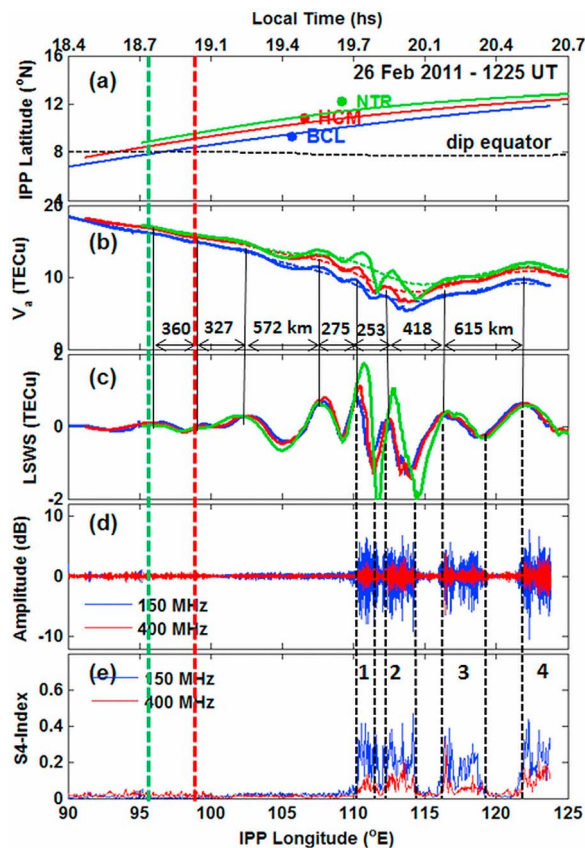
Figure 6. A typical example showing the zonal large scale wave structure and amplitude scintillations on 26 February 2011. (a) IPP tracks for three stations, BCL, HCM and NHA. (b) Longitudinal variation of V_a (solid line) and 800 km running average (dotted lines) curves for the three stations. (c) The residual TEC variations. (d) Amplitude scintillations and (e) S4-index at 150 and 400 MHz observed over BCL. The vertical green and red dotted lines represent the location of sunset terminator corresponding to E region (110 km) and F region (200) altitudes. The x axis at the top represents the local times at the corresponding longitudes.

are post-sunset hours. The residual V_a variations after subtraction of 800 km running average curves (dotted lines in Figure 6b) are shown in Figure 6c.

[16] It is interesting to observe that these zonal wave structures in the residual TEC (V_a) are closely aligned for the three stations which are separated by about 3.6° and their IPP tracks are separated by ~2.3° in dip latitude. This close alignment suggests that these zonal structures are in fact aligned with geomagnetic field ($\vec{B}$) lines at least for ~255 km since the declination angle of $\vec{B}$ lines is nearly zero in this sector. Similar alignment was also evidenced from the earlier reports by *Thampi et al.* [2009] and *Tsunoda et al.* [2010]. Figure 6d shows the amplitude scintillations observed on both 150 and 400 MHz frequency signals from BCL receiver. The similar amplitude scintillations observed from HCM and NHA receivers are not shown for simplicity. Four distinct scintillation patches, labeled 1 to 4, occurred during this particular C/NOFS pass as can be observed from Figure 6d. Most important result from this observation

is that these four scintillation patches are aligned with the westward walls of residual TEC depletions as indicated with vertical dotted lines. Since the equatorial plasma bubbles (EPBs), which cause these scintillations, are known be aligned to $\vec{B}$ field lines, it is convincing to conclude that these zonal structures are actually aligned with $\vec{B}$ field lines.

[17] It was shown that the equatorial plasma bubbles (EPBs) grow from the upwellings or crests of the LSWS [*Tsunoda and White*, 1981; *Tsunoda*, 1981, 2005]. The upwellings develop in the bottomside F region when the low-density plasma is pushed upward locally, probably due to polarization electric fields [*Weber et al.*, 1978]. This is analogous to the upwelling in fluids due to buoyancy forces. The upwellings appear as an upward push in the isoelectron density contours of incoherent scatter radar maps when viewed in East-West plane. Since the low density plasma is pushed upward, the upwellings manifest as depletions in residual TEC variations as seen in Figure 6c. *Tsunoda and White* [1981] and *Tsunoda* [1983] have further shown, from the backscatter radar maps, that the EPBs initially develop at the westward wall of upwellings. Thus, the alignment of scintillation patches with the westward walls of residual TEC depletions (Figures 6c and 6d) further reinforces the findings of earlier studies on LSWS and ESF [*Tsunoda and White*, 1981; *Tsunoda*, 1981, 1983, 2005; *Tsunoda et al.*, 2010, 2011; *Thampi et al.*, 2009]. Therefore, based on above results, (1) zonal wavelengths in the range ~250 to 615 km, (2) the alignment of EPBs (scintillation) with the westward walls of upwellings (TEC depletions), and (3) their alignment with $\vec{B}$ field lines, it can be concluded that these zonal wave-like structures observed in Figure 6 are the large scale wave structure in the bottom side F region. Thus, the differential phase measurements from the beacon transmissions from low-inclination orbiting satellites fills a void in the direct observations of LSWS, which to date, have been possible only with the ALTAIR radar.

[18] A careful examination of the Figure 6c reveals the presence of wave like feature also westward of 100°E longitude, i.e., weaker wave structure appears to be present even before the E region sunset (green dotted line). Such a sequence, namely, pre-sunset wave structure increasing in amplitude toward post-sunset hours when ESF structures may also evolve, has been reported earlier in F-layer heights by *Abdu et al.* [2009] and in TEC by *Tsunoda et al.* [2010, 2011]. This indicates that the initiation of LSWS can appear even before the sunset due to the excitation of atmospheric gravity waves (AGW) in the troposphere, their propagation up to thermosphere and transfer of AGW wind perturbations via neutral-ion coupling to the plasma at the base of F-layer [*Abdu et al.*, 2009; *Tsunoda*, 2010; *Tsunoda et al.*, 2011]. *Abdu et al.* [2009] have also reported the modulation of F-layer plasma distribution by AGW as seen in its characteristic forms in F-layer heights observed by radar and Digisonde. The substantial enhancement of LSWS amplitude during the post-sunset period indicates that the growth of LSWS is aided by the polarization electric fields developed by the F region dynamo after the sunset. The detailed discussion on the atmospheric coupling processes leading to the excitation of LSWS by AGW and the subsequent instability processes leading to the evolution of EPBs can be found in

the works by *Tsunoda* [2005, 2010], *Abdu et al.* [2009], and *Tsunoda et al.* [2010, 2011].

6. Summary and Conclusions

[19] A low-latitude network of radio beacon receivers, namely GRBR network, is currently established around the Southeast Asia and Pacific regions by the joint efforts of RISH, Kyoto University and SRI International, USA which is further planned to expand into Indian and African low latitudes. The principal experiment involves differential phase measurements at spatially distributed locations from dual/tri-band radio beacon transmitters onboard the LEOS to study the three dimensional structures of ionospheric electron content by tomographic imaging and to investigate the atmospheric coupling processes leading to the generation of ESF and scintillations. With the availability of beacon transmitters onboard the LEOS in low-inclination orbits, such as CERTO beacon on C/NOFS, it is now possible to determine the zonal (longitudinal) variation of ionospheric TEC with fine spatial resolution over a wide longitudinal region. For low-inclination satellite passes, the initial TEC offset and absolute vertical TEC can be accurately estimated using the single station observations described in section 3.2. By subtracting the background variation (zonal wavelengths > 800 km), the LSWS can be successfully extracted from the longitudinal variation of TEC. The zonal wavelengths of LSWS are found to vary around ∼250 to 615 km. These zonal structures were found, in general, to be aligned with geomagnetic ($\vec{B}$) field lines and scintillations are found to align with the westward wall of TEC depletions. The initiation of LSWS by the AGW can be observed even before the sunset and its amplitude grows substantially during the post-sunset periods, probably, aided by the polarization electric fields developed due to *F* region dynamo. These are the typical signatures of LSWS. Thus, the application of differential phase measurements for determining the longitudinal plasma structures is an excellent diagnostic tool to study the characteristics of LSWS and their source mechanisms on a regular basis. In this context, the low-latitude GRBR network lays an excellent platform to study the LSWS, scintillations and their inter-relationship to uncover the processes leading to yet enigmatic day-to-day randomness of ESF.

References

Abdu, M. A., E. A. Kherani, I. S. Batista, E. R. de Paula, D. C. Fritts, and J. H. Sobral (2009), Gravity wave initiation of equatorial spread F/plasma bubble irregularities based on observational data from the SpreadFEx campaign, *Ann. Geophys.*, *27*, 2607–2622, doi:10.5194/angeo-27-2607-2009.

Aitchison, G. J., and K. Weekes (1959), Some deductions of ionospheric information from the observations of emissions from satellites 1957a2-I, *J. Atmos. Terr. Phys.*, *14*, 236–243, doi:10.1016/0021-9169(59)90035-2.

Bernhardt, P. A., and C. L. Siefring (2006), New satellite-based systems for ionospheric tomography and scintillation region imaging, *Radio Sci.*, *41*, RS5S23, doi:10.1029/2005RS003360.

Bernhardt, P. A., C. L. Siefring, I. J. Galysh, and D. E. Koch (2010), A new technique for absolute total electron content determination using the CITRIS instrument on STPSat1 and the CERTO beacons on COSMIC, *Radio Sci.*, *45*, RS3006, doi:10.1029/2009RS004243.

Coley, W. R., R. A. Heelis, B. J. Holt, and C. R. Lippincott (2010), Ion temperature and density relationships measured by CINDI from the C/NOFS spacecraft during solar minimum, *J. Geophys. Res.*, *115*, A02313, doi:10.1029/2009JA014665.

Davies, K. (1980), Recent progress in satellite radio beacon studies with particular emphasis on the ATS-6 radio beacon experiment, *Space Sci. Rev.*, *25*, 357–430, doi:10.1007/BF00241558.

Garriott, O. K. (1960), The determination of ionospheric electron content and distribution from satellite observations: Part 1. Theory of the analysis, *J. Geophys. Res.*, *65*(4), 1139–1150, doi:10.1029/JZ065i004p01139.

Kersley, L., J. A. T. Heaton, S. E. Pryse, and T. D. Raymund (1993), Experimental ionospheric tomography with ionosonde input and EISCAT verification, *Ann. Geophys.*, *11*, 1064–1070.

Kherani, E. A., M. A. Abdu, E. R. de Paula, D. C. Fritts, J. H. A. Sobral, and F. C. de Meness Jr. (2009), The impact of gravity waves rising from convection in the lower atmosphere on the generation and nonlinear evolution of equatorial bubble, *Ann. Geophys.*, *27*, 1657–1668, doi:10.5194/angeo-27-1657-2009.

Leitinger, R., G. Schmidt, and A. Tauriainen (1975), An evaluation method combining the differential Doppler measurements from two stations that enables the calculation of electron content of the ionosphere, *J. Geophys.*, *41*, 201–213.

Oppenheim, A. V., and R. W. Schafer (1989), Design of FIR filters by Windowing, in *Discrete-Time Signal Processing*, pp. 447–448, Prentice Hall, Englewood Cliffs, N. J.

Rottger, J. (1973), Wave-like structures of large-scale equatorial spread-F irregularities, *J. Atmos. Terr. Phys.*, *35*, 1195–1206, doi:10.1016/0021-9169(73)90016-0.

Saito, S., and T. Maruyama (2007), Large-scale longitudinal variation in ionospheric height and equatorial spread F occurrences observed by ionosondes, *Geophys. Res. Lett.*, *34*, L16109, doi:10.1029/2007GL030618.

Singh, S., F. S. Johnson, and R. A. Power (1997), Gravity wave seeding of equatorial plasma bubbles, *J. Geophys. Res.*, *102*, 7399–7410, doi:10.1029/96JA03998.

Thampi, S. V., M. Yamamoto, R. T. Tsunoda, Y. Otsuka, T. Tsugawa, J. Uemoto, and M. Ishii (2009), First observations of large-scale wave structure and equatorial spread F using CERTO radio beacon on the C/NOFS satellite, *Geophys. Res. Lett.*, *36*, L18111, doi:10.1029/2009GL039887.

Tsunoda, R. T. (1981), Time evolution and dynamics of equatorial backscatter plumes, 1. Growth Phase, *J. Geophys. Res.*, *86*, 139–149, doi:10.1029/JA086iA01p00139.

Tsunoda, R. T. (1983), On the generation and growth of equatorial backscatter plumes: 2. Structuring of the west walls of upwellings, *J. Geophys. Res.*, *88*, 4869–4874, doi:10.1029/JA088iA06p04869.

Tsunoda, R. T. (2005), On the enigma of day-to-day variability in equatorial spread F, *Geophys. Res. Lett.*, *32*, L08103, doi:10.1029/2005GL022512.

Tsunoda, R. T. (2008), Satellite traces: An ionogram signature for large-scale wave structure and a precursor for equatorial spread F, *Geophys. Res. Lett.*, *35*, L20110, doi:10.1029/2008GL035706.

Tsunoda, R. T. (2010), On equatorial spread F: Establishing a seeding hypothesis, *J. Geophys. Res.*, *115*, A12303, doi:10.1029/2010JA015564.

Tsunoda, R. T., and D. M. Towle (1979), On the spatial relationship of 1-meter equatorial spread-F irregularities and depletions in total electron content, *Geophys. Res. Lett.*, *6*, 873–876, doi:10.1029/GL006i011p00873.

Tsunoda, R. T., and B. R. White (1981), On the generation and growth of equatorial backscatter plumes: 1. Wave structure in the bottomside F layer, *J. Geophys. Res.*, *86*, 3610, doi:10.1029/JA086iA05p03610.

Tsunoda, R. T., D. M. Bubenik, S. V. Thampi, and M. Yamamoto (2010), On large-scale wave structure and equatorial spread F without a post-sunset rise of the F layer, *Geophys. Res. Lett.*, *37*, L07105, doi:10.1029/2009GL042357.

Tsunoda, R. T., M. Yamamoto, T. Tsugawa, T. L. Hoang, S. Tulasi Ram, S. V. Thampi, H. D. Chau, and T. Nagatsuma (2011), On seeding, large-scale wave structure, equatorial spread F, and scintillations over Vietnam, *Geophys. Res. Lett.*, *38*, L20102, doi:10.1029/2011GL049173.

Tulasi Ram, S., S.-Y. Su, C. H. Liu, B. W. Reinisch, and L.-A. McKinnell (2009), Topside ionospheric effective scale heights (HT) derived with ROCSAT-1 and ground-based ionosonde observations at equatorial and midlatitude stations, *J. Geophys. Res.*, *114*, A10309, doi:10.1029/2009JA014485.

Weber, E. J., J. Buchau, R. H. Eather, and S. B. Mende (1978), North-south aligned equatorial airglow depletions, *J. Geophys. Res.*, *83*, 712–716, doi:10.1029/JA083iA02p00712.

Yamamoto, M. (2008), Digital beacon receiver for ionospheric TEC measurement developed with GNU radio, *Earth Planets Space*, *60*, e21–e24.

S. Gurubaran, Equatorial Geophysical Research Laboratory, Indian Institute of Geomagnetism, Tirunelveli 627 011, India.

S. V. Thampi, Physical Research Laboratory, Ahmedabad, Gujarat 380009, India.

R. T. Tsunoda, Center for Geospace Studies, SRI International, 333 Ravenswood Ave., Menlo Park, CA 94025, USA.

S. Tulasi Ram and M. Yamamoto, RISH, Kyoto University, Uji, Kyoto 611-0011, Japan. (tulasi@rish.kyoto-u.ac.jp)